Applied Physics Letters

RESEARCH ARTICLE | JUNE 29 2023

A WSe_2/β-Ga_2O_3 2D/3D heterojunction for self-powered solar-blind communication

Xin Zhou; Zhang Jinzhong (张金中); Shang Liyan (商丽燕); Li Yawei (李亚巍); Zhu Liangqing (朱亮清); Chu Junhao (褚君浩); Hu Zhigao (胡志高)

Appl. Phys. Lett. 122, 263509 (2023)
https://doi.org/10.1063/5.0145228

AIP Publishing

A WSe_2/β-Ga_2O_3 2D/3D heterojunction for self-powered solar-blind communication

Cite as: Appl. Phys. Lett. **122**, 263509 (2023); doi: 10.1063/5.0145228
Submitted: 3 February 2023 · Accepted: 9 June 2023 ·
Published Online: 29 June 2023

View Online Export Citation CrossMark

Xin Zhou,[1] Jinzhong Zhang (张金中),[1,a)] Liyan Shang (商丽燕),[1] Yawei Li (李亚巍),[1] Liangqing Zhu (朱亮清),[1] Junhao Chu (褚君浩),[1] and Zhigao Hu (胡志高)[1,2,b)]

AFFILIATIONS

[1]Technical Center for Multifunctional Magneto-Optical Spectroscopy (Shanghai), Engineering Research Center of Nanophotonics and Advanced Instrument (Ministry of Education), Department of Physics, School of Physics and Electronic Science, East China Normal University, Shanghai 200241, China
[2]Collaborative Innovation Center of Extreme Optics, Shanxi University, Taiyuan, Shanxi 030006, China

[a)]Electronic mail: jzzhang@ee.ecnu.edu.cn
[b)]Author to whom correspondence should be addressed: zghu@ee.ecnu.edu.cn

ABSTRACT

Self-powered flexible solar-blind photodetectors based on WSe_2/β-Ga_2O_3 2D/3D van der Waals (vdW) heterojunctions were manufactured, which exhibit brilliant optoelectronic performances with a low dark current of 136 fA at 0 V, a I_{254nm}/I_{dark} ratio of 10^3, and rise ($\tau_r = 9$ ms) and decay ($\tau_d = 18$ ms) times. In a further step, a solar-blind communication system was fabricated with a good information transmission capability and low energy consumption. Furthermore, "AND" and "OR" optoelectronic logic gates have been realized, which can be applied to signal processing in the field of solar-blind communication.

Radio frequency (RF) and optical communication systems are widely used in military and commercial wireless communication fields.[1–9] Compared with RF communication, optical communication has the advantages such as bigger bandwidth, lower power-consumption, higher power densities, smaller size, etc.[10] Optical communication systems transmit information through optical signals with a wavelength range from infrared (IR) to ultraviolet (UV). IR technology has been reported to be used in wireless communication systems.[1,11] However, solar radiation and fluorescence noise will interfere with IR detectors, which limits the development of IR wireless communication.[10] Fortunately, the communication system based on UVC (280–100 nm) could overcome the above challenges since the UVC radiation is almost absorbed by ozone and cannot reach the earth surface (i.e., solar-blind).[2] In addition, UV links can be used in combination with optical or RF links.[10] The solar-blind photodetectors (SBPDs) based on Ga_2O_3,[2–4] AlN,[12] GaN,[13–15] AlGaN,[16–18] and diamond[9] are used as the signal receivers of the solar-blind communication systems. Among them, Ga_2O_3 has attracted intensive attention due to an ultra-wideband gap ($\sim$4.9 eV), high critical breakdown field ($\sim$8 MV/cm), high electron mobility, high chemical/thermal stability, simple preparation process, etc.[2–4]

Fabricating heterostructures is an effective method to improve the optoelectronic performance of the SBPDs. It is reported that the β-Ga_2O_3/WO_3 heterojunction exhibits record low noise with ultralow dark current of 6.5 fA, $I_{254\,nm}/I_{dark}$ ratio of 6.4×10^5, and rise/decay time of 168 ms/171 ms at 0 V.[19] Zhao *et al.* reported that the Ga_2O_3/Bi_2Se_3 heterojunction presents a low dark current of 3.12 pA, detectivity of 6.2×10^{13} Jones, and an ultrafast rise (0.6 ms) and decay (1.2 ms) response time.[20] Unfortunately, defects and dislocations in traditional 3D/3D heterostructures are easily generated due to lattice mismatch and incompatible crystal structure.[21] In order to overcome the challenge, 2D/3D mixed-dimensional vdW heterostructures have been fabricated. For example, the $PtSe_2/\beta$-Ga_2O_3 heterojunction achieves a high responsivity of 76.2 mA/W, a large on/off current ratio of 10^5, and an ultrafast response time of 12 μs.[22] The $GaSe/Ga_2O_3$ vertical heterojunction shows a nonlinear rectifying characteristic with a high rectification ratio of 2500, specific detectivity of 1.6×10^{11} Jones, and photoresponsivity of 70 mA/W.[21] Flexibility, portability, and wearability are important development directions of next generation optoelectronic devices, and various flexible optoelectronic devices have been developed.[23,24] In our previous work, a stamp-based printing technique was applied to transfer the β-Ga_2O_3 films grown by pulsed laser deposition (PLD) from Si substrates onto flexible PET (polyethylene terephthalate) substrates. It is demonstrated that the β-Ga_2O_3-based flexible SBPDs exhibit brilliant optoelectronic performances with a low dark current (1.7 pA) at 10 V and a high $I_{254\,nm}/I_{dark}$ ratio ($>10^3$).[24] However, flexible SBPDs based on 2D/3D mixed-dimensional vdW heterojunctions are rarely reported.

In this work, self-powered flexible SBPDs based on WSe_2/β-Ga_2O_3 2D/3D vdW heterojunctions were manufactured, which exhibit brilliant optoelectronic performances and stability under different bending stresses. In a further step, a solar-blind communication system was fabricated, which demonstrates a good information transmission capability and low energy consumption. Finally, "AND" and "OR" optoelectronic logic gates (OELGs) have been realized with accurate signal processing capability, which can be applied in the field of solar-blind communication.

The β-Ga_2O_3 films (∼186 nm) were grown on Si(100) substrates by PLD and then transferred onto flexible PET substrates by a stamp-based printing technique. More details can be found in Refs. 24 and 25. The 100 nm-thick Au pads were deposited on β-Ga_2O_3 films by a thermal evaporator with a mask. The WSe_2 flakes were mechanically exfoliated from the bulk single crystal by a scotch tape, and then it was transferred onto the β-Ga_2O_3 films with the help of polydimethylsiloxane (PDMS). Electron beam lithography (EBL, Pioneer Two, Raith) was used to realize electrode patterns on WSe_2 flakes. After developing, Ni/Au (2/50 nm) electrodes were thermally evaporated onto the WSe_2 flakes. Due to process difficulties, we did not insert an insulating spacer between β-Ga_2O_3 and the metal electrode, resulting in a parallel current path. The optoelectronic performance of the self-powered flexible SBPDs based on WSe_2/β-Ga_2O_3 2D/3D vdW heterojunctions was tested by an accurate semiconductor parameter analyzer (Keithley 4200-SCS) with a 254 nm-light source.

As shown in Fig. 1(a), the x-ray diffraction peaks of the as-deposited Ga_2O_3 films nearby 18.9°, 38.4°, and 59.1° correspond to the ($\bar{2}01$), ($\bar{4}02$), and ($\bar{6}03$) crystal planes (JCPDF Card: No. 43-1012), respectively.[24] It indicates that the Ga_2O_3 films transferred from Si onto PET substrates are polycrystalline with the β phase. The typical Raman spectra of WSe_2 sheets consist of two main phonon vibration modes, which can be assigned to the E^1_{2g} (247 cm^{-1}) and A_{1g} (254 cm^{-1}) modes.[26] The characteristic peak of β-Ga_2O_3 at 200 cm^{-1} is assigned to the A^3_g Raman-active mode [cf. Fig. 1(b)]. The PL spectra [Fig. 1(c)] show a peak at 751 nm, indicating a bandgap value of 1.65 eV. Figure 1(d) is the SEM image of a WSe_2/β-Ga_2O_3 2D/3D vdW heterojunction (scale bar: 5 μm). The area enclosed by green dots is a WSe_2 sheet, and the areas enclosed by yellow dashes are Ni/Au electrodes. According to the corresponding EDS elements mappings images exhibited in Fig. 1(e), W and Se elements are only located on the mechanically exfoliated flake, while Ga and O elements are distributed on the whole substrate surface. The results indicate the formation of WSe_2/β-Ga_2O_3 2D/3D vdW heterojunctions.

Kelvin probe force microscopic (KPFM) was employed to further understand the band structure of the WSe_2/β-Ga_2O_3 heterojunction. Figure 2(a) shows the AFM topography of a lateral WSe_2/β-Ga_2O_3 heterostructure, and the thickness of the WSe_2 flake is about 9.26 nm (∼12 layers). The contact potential difference (CPD) between the probe tip and the sample surface can be expressed as[27]

$$\begin{aligned} CPD_{WSe_2} &= (W_{tip} - W_{WSe_2})/e, \\ CPD_{Ga_2O_3} &= (W_{tip} - W_{Ga_2O_3})/e, \end{aligned} \tag{1}$$

where W_{tip}, W_{WSe_2}, and $W_{Ga_2O_3}$ are the surface work function of the KPFM probe tip, WSe_2, and Ga_2O_3, respectively. The distinction between the Fermi levels of WSe_2 and β-Ga_2O_3 can be calculated from the CPD difference:[28] $\Delta E_F = E_{F_{WSe_2}} - E_{F_{Ga_2O_3}} = e(CPD_{WSe_2} - CPD_{Ga_2O_3})$. The surface potential distribution was fitted by the sigmoidal function as shown in Fig. 2(b). It indicates that the work function of WSe_2 is 0.3 eV larger than that of β-Ga_2O_3. Hence, the work function difference is 0.3 eV, which is similar to previous reports ($W_{WSe_2} = 4.4$ eV, $W_{Ga_2O_3} = 4.1$ eV).[29,30] The lateral depletion region width can be estimated as 650 nm. Furthermore, the distribution of built-in electric field can be obtained by differentiating the sigmoid fitting profile

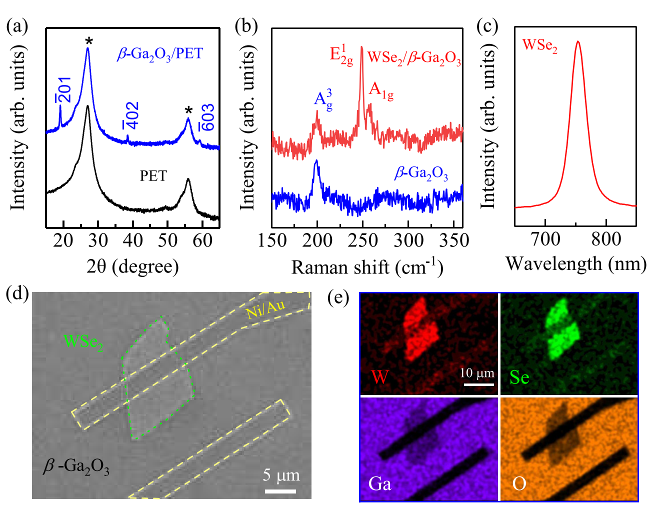

FIG. 1. (a) XRD of the PET and β-Ga_2O_3/PET. (b) Raman spectra of the β-Ga_2O_3/PET and WSe_2/β-Ga_2O_3/PET. (c) PL spectra of the WSe_2/β-Ga_2O_3/PET. (d) SEM image and (e) corresponding EDS elements (W, Se, Ga, and O) mappings images of the WSe_2/β-Ga_2O_3 2D/3D vdW heterojunction.

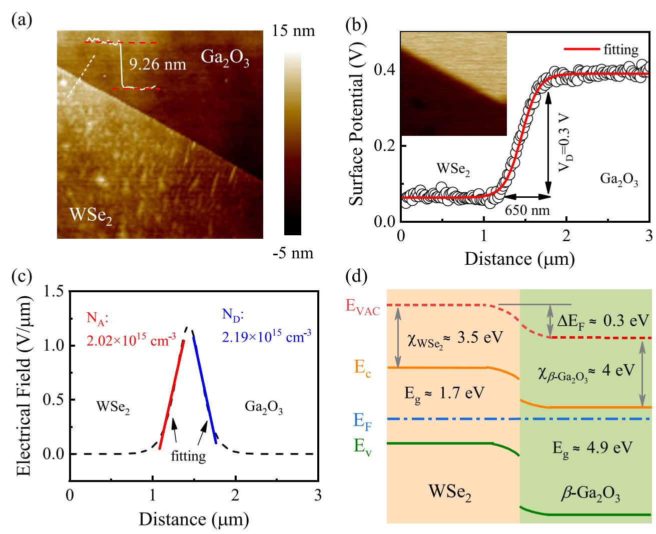

FIG. 2. (a) An AFM image (scanning range: 4×4 μm) and (b) the corresponding surface potential distribution. Inset: KPFM image. (c) Built-in electric field distribution and (d) the energy-band diagram of a WSe_2/β-Ga_2O_3 2D/3D vdW heterojunction.

($\xi = -\nabla\varphi$). As an abrupt junction, the built-in electric field $\xi(x)$ can be defined as follows:[31]

$$\xi_{WSe_2}(x) = \frac{qN_A(x - x_p)}{\varepsilon_{WSe_2}\varepsilon_0} \quad (x_p < x < x_0),$$
$$\xi_{Ga_2O_3}(x) = \frac{qN_D(x_n - x)}{\varepsilon_{Ga_2O_3}\varepsilon_0} \quad (x_0 < x < x_n), \tag{2}$$

where ε_0 is the vacuum permittivity. The ε_{WSe_2} and $\varepsilon_{Ga_2O_3}$ are the relative permittivities of the WSe_2 and β-Ga_2O_3, whose values are 11.7 and 10.2, respectively.[31,32] N_A and N_D are the carrier concentration of the WSe_2 and β-Ga_2O_3 derived by linearly fitting the built-in electric field distribution. The values are 2.02×10^{15} cm^{-3} and 2.19×10^{15} cm^{-3}, respectively, which are within a reasonable range compared to previous reports (WSe_2: 2.99×10^{14} cm^{-3} and Ga_2O_3: 3.1×10^{16} cm^{-3}).[21,31] In addition, the maximum electric field is estimated to be 1.2 V/μm. The x_p, x_0, and x_n are the boundaries of the depletion layer. Meanwhile, the total depletion width (W_D) and each depletion width in the WSe_2 (W_p) and β-Ga_2O_3 (W_n) can be calculated as follows:[28]

$$W_D = \sqrt{\frac{2\varepsilon_{WSe_2}\varepsilon_{Ga_2O_3}\varepsilon_0(N_A + N_D)^2 V_D}{qN_A N_D(\varepsilon_{WSe_2}N_A + \varepsilon_{Ga_2O_3}N_D)}},$$
$$W_p = \sqrt{\frac{2\varepsilon_{WSe_2}\varepsilon_{Ga_2O_3}\varepsilon_0 N_D V_D}{qN_A(\varepsilon_{WSe_2}N_A + \varepsilon_{Ga_2O_3}N_D)}}, \tag{3}$$
$$W_n = \sqrt{\frac{2\varepsilon_{WSe_2}\varepsilon_{Ga_2O_3}\varepsilon_0 N_A V_D}{qN_D(\varepsilon_{WSe_2}N_A + \varepsilon_{Ga_2O_3}N_D)}}.$$

The calculation results show that $W_p = 302$, $W_n = 278$, and $W_D = 580$ nm, which is consistent with the previous estimated results. The energy-band diagram is shown in Fig. 2(d), which presents a type-II band alignment at the interface of the heterojunction.[26] Due to the difference between the Fermi levels, the electrons diffuse from β-Ga_2O_3 to WSe_2, causing hole accumulation (i.e., acceptor state) on the Ga_2O_3 side with an upward band bending and electron accumulation (i.e., donor state) on the WSe_2 side with a downward band bending.[33] When the heterojunction is exposed to UVC light, electron–hole pairs are generated and then quickly separated by the built-in electric field, resulting in a large photocurrent and fast response.

Responsivity (R) is an important parameter for SBPDs, which is defined as $R = I_{photo}/(P_{in} \times S)$. Here, I_{photo} is the photocurrent, P_{in} is the power density of the incident light, and S is the effective working area of SBPD.[3] In Fig. 3(a), the response spectrum of the SBPDs reveals that the response wavelength region is about 200–280 nm, which coincides with the solar-blind region. In Fig. 3(b), the I–V curves of the WSe_2/β-Ga_2O_3 2D/3D vdW heterojunctions under dark condition exhibit a typical rectification characteristic with a rectification ratio of about 50 at ±5 V. At the bias voltage of 0 V, the flexible SBPDs based on WSe_2/β-Ga_2O_3 2D/3D vdW heterojunctions have a low dark current (I_{dark}) of 136 fA, a I_{254nm}/I_{dark} ratio of about 10^3, and an open circuit voltage (V_{OC}) of about 0.2 V, which indicates the photovoltaic effect and self-powered operation of the SBPDs.[19] The rise/decay time of the SBPD is defined as the current increases/decreases from 10% to 90% or from 90% to 10%, as shown in Fig. 3(c). It reveals that the SBPDs have a fast response with rise ($\tau_r = 9$ ms) and decay ($\tau_d = 18$ ms) times. Figure 3(d) depicts that I_{photo} increases as the power density of incident light (P_{in}) increases since more carriers are generated. Due to the trapping and detrapping effects caused by interface states, anomalous transient photocurrent behaviors can be observed at large P_{in}.[34–36] As shown in Fig. 3(e), the I_{254nm} and I_{dark} are almost unchange during repeated bending between 0° and 180°, which indicates that the SBPDs work stably under strains of 0%–0.31% (measured by a strain gauge). Table I shows a comparison of our work with some other Ga_2O_3-based flexible SBPDs.

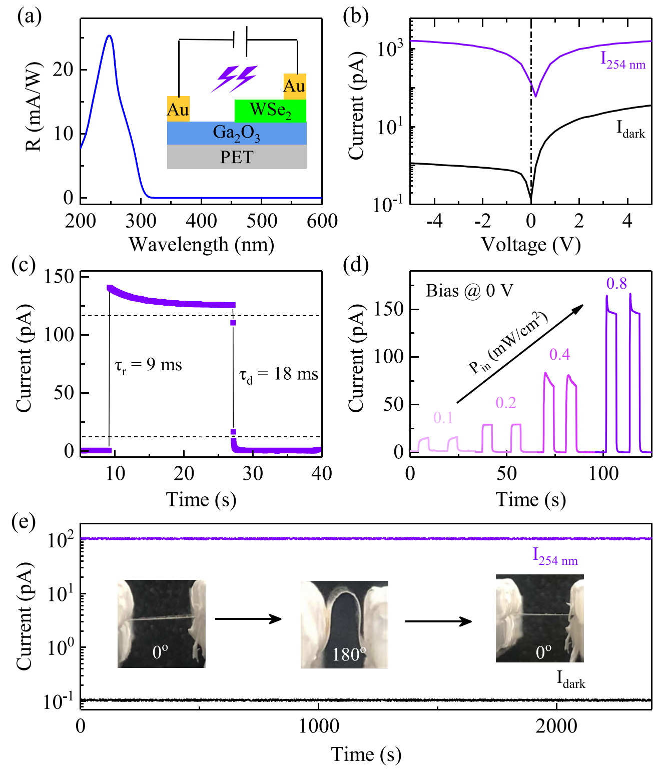

FIG. 3. (a) Response spectrum of a SBPD based on the WSe_2/β-Ga_2O_3 2D/3D vdW heterojunction as a function of illumination wavelength. Inset: the diagram of a SBPD. (b) I–V and (c) I–t curves of the SBPD under dark condition or UVC illumination ($\lambda = 254$ nm). (d) I–t curves at different pulsed light power densities of $P_{in} = 0.1$, 0.2, 0.4, and 0.8 mW/cm^2. (e) I–t curves at different bending states (more than 1000 bending cycles). Inset: photographs of single bending cycle from 0° to 180° and back to 0°.

TABLE I. Comparison of the key parameters of flexible Ga_2O_3-based PDs.

Substrate material	Active material	I_{dark} (pA)	ON/OFF ratio	R (A/W)	τ_r (ms)
PET[a]	β-Ga_2O_3/WSe_2	0.1	$\sim 10^3$	0.03	9
Mica[37]	β-Ga_2O_3/MoS_2	2	$\sim 10^3$	0.02	700
Hastelloy[38]	β-Ga_2O_3/NiO	10	$\sim 10^2$	0.6	490
Mica[39]	β-Tm:Ga_2O_3	36	$\sim 10^3$	0.4	20
PET[24]	β-Ga_2O_3	1.7	$\sim 10^3$	0.9	90
PEN[40]	a-Ga_2O_3	6	$\sim 10^4$	$<10^{-3}$	0.2
PI[41]	a-Ga_2O_3/PbI_2	0.1	$\sim 10^4$	0.1	2
Mica[42]	a-Ga_2O_3/ZnO	$> 10^3$	<10	12	$>10^3$

[a]This work.

In a further step, a solar-blind communication system has been fabricated, and the self-powered SBPDs based on WSe_2/β-Ga_2O_3 2D/3D vdW heterojunctions are used as the signal receivers, as illustrated in Fig. 4(a). In Fig. 4(b), the "ECNU" is transferred to test the solar-blind communication system. The input signals encrypted by Morse code were sent by the UVC light source (254 nm, 0.8 mW/cm^2) with a shutter and then transmitted wirelessly in the free space. Finally, the signals were recognized by the SBPDs. Note that the signals are composed of dots (·) and dashes (-). The time length of a dash is three times than that of a dot. Within a word, the interval between each dot or/and dash is the time length of a dot. On the other hand, the interval is the time length of seven dots between different words.[43] The "ECNU" can be clearly recognized after decoding, which means that the solar-blind communication system has excellent information transmission capability and low energy consumption.

In order to further study the potential application of SBPD in optoelectronic logic operation, the "AND" and "OR" optoelectronic logic gates were manufactured [cf. Fig. 5(a)]. The light source OFF and ON are defined as logic "0" and "1" of the input signals, respectively. Correspondingly, $I < 5$ pA and $I > 50$ pA represent logic "0" and "1" of the output signals, respectively. The truth table of OELGs is shown in Fig. 5(b). For the case of "AND" OELG, two SBPDs are arranged in series. The current in the circuit will be larger than 50 pA only when both SBPDs are illuminated by UVC. The corresponding output current is shown in Fig. 5(c). For the case of "OR" OELG, two SBPDs are arranged in parallel. The current in the circuit will be larger than 50 pA when one or both SBPDs are exposed to UVC. The corresponding output current is shown in Fig. 5(d). The OELGs demonstrate accurate signal processing capability, which may be applied in the field of solar-blind communication.

In summary, self-powered flexible SBPDs based on WSe_2/β-Ga_2O_3 2D/3D vdW heterojunctions were manufactured, which exhibit brilliant optoelectronic performances with a low dark current of 136 fA at 0 V, a I_{254nm}/I_{dark} ratio of 10^3, and rise ($\tau_r = 9$ ms) and decay ($\tau_d = 18$ ms) times. In a further step, solar-blind communication system was fabricated, which demonstrates a good information transmission capability and low energy consumption. Furthermore, the "AND" and "OR" OELGs have been realized with an accurate signal processing capability.

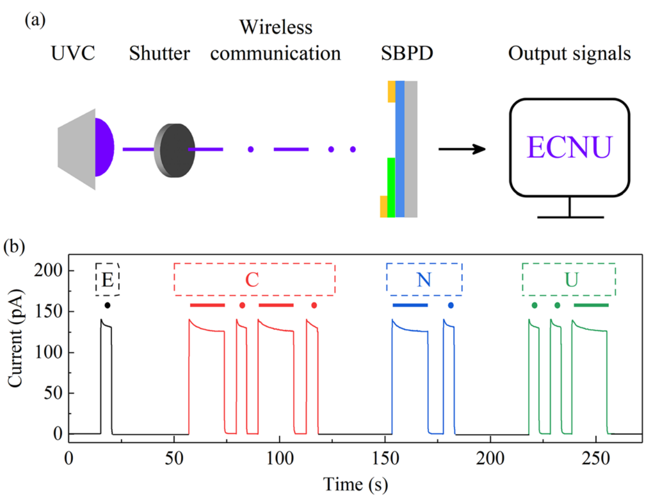

FIG. 4. (a) Schematic diagram of a solar-blind communication system. (b) The output signals encrypted by Morse code "ECNU," which are the current value of the SBPDs.

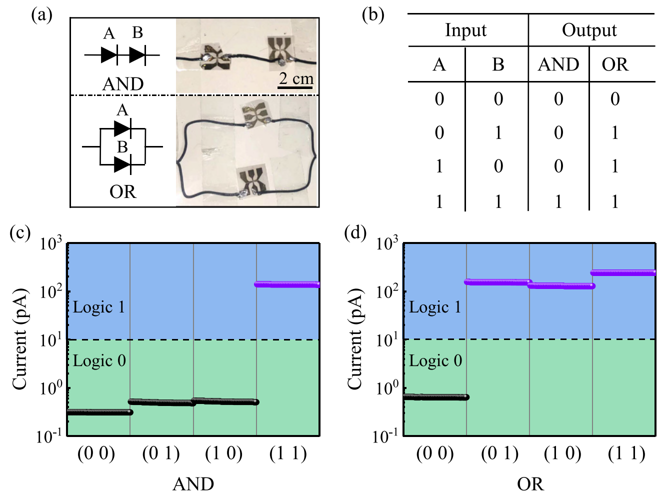

Input		Output	
A	B	AND	OR
0	0	0	0
0	1	0	1
1	0	0	1
1	1	1	1

FIG. 5. (a) Schematic diagram and the corresponding photograph of the "AND" and "OR" optoelectronic logic gates. (b) Truth table of the "AND" and "OR" gates. The I–t curves of (c) "AND" and (d) "OR" gates in response to different input signals (AB).

This work was supported in part by the National Key Research and Development Program of China (Grant No. 2019YFB2203403), the National Natural Science Foundation of China (Grant Nos. 62090013, 62074058, 61974043, and 61974044), the Projects of Science and Technology Commission of Shanghai Municipality (Grant No. 21JC1402100), and the Program for Professor of Special Appointment (Eastern Scholar) at Shanghai Institutions of Higher Learning.

AUTHOR DECLARATIONS

Conflict of Interest

The authors have no conflicts to disclose.

Author Contributions

Xin Zhou: Data curation (lead); Formal analysis (lead); Methodology (equal). **Jinzhong Zhang:** Formal analysis (equal); Investigation (equal). **Liyan Shang:** Formal analysis (supporting); Investigation (supporting). **Y. W. Li:** Formal analysis (supporting); Investigation (supporting). **Liangqing Zhu:** Data curation (supporting). **Junhao Chu:** Supervision (equal). **Zhigao Hu:** Conceptualization (lead); Project administration (lead); Supervision (lead); Writing – review & editing (equal).

DATA AVAILABILITY

The data that support the findings of this study are available from the corresponding author upon reasonable request.

REFERENCES

[1]T. Mueller, F. Xia, and P. Avouris, Nat. Photonics **4**, 297 (2010).
[2]Y. Chen, X. Yang, C. Zhang, G. He, X. Chen, Q. Qiao, J. Zang, W. Dou, P. Sun, Y. Deng, L. Dong, and C. X. Shan, Nano Lett. **22**, 4888 (2022).
[3]C. Wu, F. Wu, C. Ma, S. Li, A. Liu, X. Yang, Y. Chen, J. Wang, and D. Guo, Mater. Today Phys. **23**, 100643 (2022).
[4]S. Zhou, X. Peng, H. Liu, Z. Zhang, L. Ye, H. Li, Y. Xiong, L. Niu, F. Chen, L. Fang, C. Kong, W. Li, X. Yang, and H. Zhang, Opt. Mater. Express **12**, 327 (2022).
[5]X. Zhang, X. Liu, B. Sun, H. Ye, C. He, L. Kong, T. Shi, G. Liao, and Z. Liu, ACS Appl. Mater. Interfaces **13**, 44509 (2021).
[6]H. Fang, C. Zheng, L. Wu, Y. Li, J. Cai, M. Hu, X. Fang, R. Ma, Q. Wang, and H. Wang, Adv. Funct. Mater. **29**, 1809013 (2019).
[7]C. H. Kang, I. Dursun, G. Liu, L. Sinatra, X. Sun, M. Kong, J. Pan, P. Maity, E. N. Ooi, T. K. Ng, O. F. Mohammed, O. M. Bakr, and B. S. Ooi, Light Sci. Appl. **8**, 94 (2019).
[8]M. Kumar, J. Y. Park, and H. Seo, ACS Appl. Mater. Interfaces **13**, 12241 (2021).
[9]C. Lin, Y. Lu, Y. Tian, C. Gao, M. Fan, X. Yang, L. Dong, and C. Shan, Opt. Express **27**, 29962 (2019).
[10]Z. Xu and B. M. Sadler, IEEE Commun. Mag. **46**, 67 (2008).
[11]D. Schall, D. Neumaier, M. Mohsin, B. Chmielak, J. Bolten, C. Porschatis, A. Prinzen, C. Matheisen, W. Kuebart, B. Junginger, W. Templ, A. L. Giesecke, and H. Kurz, ACS Photonics **1**, 781 (2014).
[12]N. Liu, T. Zhang, L. Chen, J. Zhang, S. Hu, W. Guo, W. Zhang, and J. Ye, IEEE Electron Device Lett. **43**, 68 (2022).
[13]Y. Ma, T. Chen, X. Zhang, W. Tang, B. Feng, Y. Hu, L. Zhang, X. Zhou, X. Wei, K. Xu, D. Mudiyanselage, H. Fu, and B. Zhang, ACS Appl. Mater. Interfaces **14**, 35194 (2022).
[14]B. Feng, H. Lv, J. Liu, R. Chen, H. Zhu, X. Han, C. Luan, and H. Xiao, Appl. Surf. Sci. **604**, 154505 (2022).
[15]G. Wu, L. Tang, G. Deng, L. Liu, Q. Hao, S. Yuan, J. Wang, H. Wei, Y. Zhao, B. Yue, J. Shi, Y. Tan, R. Li, Y. Zhang, J. Yan, X. Yi, J. Wang, J. Kong, and J. Li, Opt. Express **30**, 21349 (2022).
[16]Y. Gao, J. Yang, X. Ji, R. He, J. Yan, J. Wang, and T. Wei, ACS Appl. Mater. Interfaces **14**, 21232 (2022).
[17]Q. Wen, C. Wang, X. Qiu, Z. Lv, and H. Jiang, Appl. Surf. Sci. **591**, 153144 (2022).
[18]D. Wang, X. Liu, S. Fang, C. Huang, Y. Kang, H. Yu, Z. Liu, H. Zhang, R. Long, Y. Xiong, Y. Lin, Y. Yue, B. Ge, T. K. Ng, B. S. Ooi, Z. Mi, J. H. He, and H. Sun, Nano Lett. **21**, 120 (2021).
[19]S. Li, J. Yue, C. Wu, Z. Liu, Z. Yan, P. Li, D. Guo, Z. Wu, Y. Guo, and W. Tang, IEEE Sens. J. **21**, 26724 (2021).
[20]B. Zhao, K. Li, Q. Liu, and X. Liu, IEEE Trans. Electron Devices **69**, 1894 (2022).
[21]S. Sorifi, S. Kaushik, H. Sheoran, and R. Singh, J. Phys. D: Appl. Phys. **55**, 365105 (2022).
[22]D. Wu, Z. Zhao, W. Lu, L. Rogée, L. Zeng, P. Lin, Z. Shi, Y. Tian, X. Li, and Y. H. Tsang, Nano Res. **14**, 1973 (2021).
[23]Y. Wang, Z. Yang, H. Li, S. Li, Y. Zhi, Z. Yan, X. Huang, X. Wei, W. Tang, and Z. Wu, ACS Appl. Mater. Interfaces **12**, 47714 (2020).
[24]X. Zhou, M. Li, J. Z. Zhang, L. Y. Shang, K. Jiang, Y. W. Li, L. Q. Zhu, J. H. Chu, and Z. G. Hu, IEEE Electron Device Lett. **43**, 1921 (2022).
[25]X. Zhou, M. Li, J. Z. Zhang, L. Y. Shang, K. Jiang, Y. W. Li, L. Q. Zhu, Z. G. Hu, and J. H. Chu, IEEE Electron Device Lett. **43**, 580 (2022).
[26]J. Kim, M. A. Mastro, M. J. Tadjer, and J. Kim, ACS Appl. Mater. Interfaces **10**, 29724 (2018).
[27]H. Ji, M. Z. Xie, J. Y. Zhou, X. Wang, Z. Jin, K. Jiang, L. Y. Shang, Z. G. Hu, and J. H. Chu, Appl. Phys. Lett. **115**, 162104 (2019).
[28]J. Y. Zhou, M. Z. Xie, H. Ji, A. Y. Cui, Y. Ye, K. Jiang, L. Y. Shang, Z. G. Hu, and J. H. Chu, ACS Appl. Mater. Interfaces **12**, 18674 (2020).
[29]M. Mohamed, K. Irmscher, C. Janowitz, Z. Galazka, R. Manzke, and R. Fornari, Appl. Phys. Lett. **101**, 132106 (2012).
[30]Z. Cui, X. Ke, E. Li, X. Wang, Y. Ding, T. Liu, M. Li, and B. Zhao, Opt. Quantum Electron. **50**, 1 (2017).
[31]T. Jiang, F. Wang, A. Y. Cui, S. Guo, K. Jiang, L. Y. Shang, Z. G. Hu, and J. H. Chu, Nanotechnology **29**, 435703 (2018).
[32]B. Liu, M. Gu, and X. Liu, Appl. Phys. Lett. **91**, 172102 (2007).
[33]M. Mishra, A. Gundimeda, T. Garg, A. Dash, S. Das, Vandana, and G. Gupta, Appl. Surf. Sci. **478**, 1081 (2019).
[34]H. Tian, A. Hu, Q. Liu, X. He, and X. Guo, Adv. Opt. Mater. **8**, 1901741 (2020).
[35]C. R. McNeill, I. Hwang, and N. C. Greenham, J. Appl. Phys. **106**, 024507 (2009).
[36]L. Hu, X. Liu, S. Dalgleish, M. M. Matsushit, H. Yoshikawab, and K. Awaga, J. Mater. Chem. C **3**, 5122 (2015).
[37]M. Sharma, A. Singh, A. Kapoor, A. Singh, B. R. Tak, S. Kaushik, S. Bhattacharya, and R. Singh, ACS Appl. Electron. Mater. **5**, 2296 (2023).
[38]X. Tang, Y. Lu, R. Lin, C. Liao, Y. Zhao, K. Li, N. Xiao, H. Cao, W. Babatain, and X. Li, Appl. Phys. Lett. **122**, 121101 (2023).
[39]Q. Qu, Q. Liu, L. Chen, Y. Li, H. Pan, J. Chen, M. Li, Y. Lu, and Y. He, Appl. Phys. Lett. **120**, 122108 (2022).
[40]C. Hsu, R. Zhu, P. Kang, P. Gao, W. Wu, D. Wuu, S. Lien, and W. Zhu, Mater. Lett. **340**, 134204 (2023).
[41]J. Zhang, F. Liu, D. Liu, Y. Yin, M. Wang, Z. Sa, L. Sun, X. Zheng, X. Zhuang, Z. Lv, W. Mu, Z. Jia, Y. Tan, F. Chen, and Z. Yang, Mater. Today Phys. **31**, 100997 (2023).
[42]J. Wang, Y. Zhou, Z. Wang, B. Wang, Y. Li, B. Wu, C. Hao, Y. Zhang, and H. Zheng, Nanoscale **15**, 7068 (2023).
[43]B. Gold, IRE Trans. Inf. Theory **5**, 17 (1959).